Research Article

Gene and protein expression profiles of olfactory ensheathing cells from olfactory bulb *versus* olfactory mucosa

https://doi.org/10.4103/1673-5374.317986

Date of submission: November 25, 2020

Date of decision: March 8, 2021

Date of acceptance: May 12, 2021

Date of web publication: July 8, 2021

Yuan-Xiang Lan[1, 2, 3, #], Ping Yang[4, #], Zhong Zeng[1, 2, 3], Neeraj Yadav[3, 5], Li-Jian Zhang[1, 2, 3], Li-Bin Wang[6, *], He-Chun Xia[2, 3, *]

Graphical Abstract *Olfactory ensheathing cells from the olfactory bulb and olfactory mucosa differ at the transcriptomic and proteomic levels*

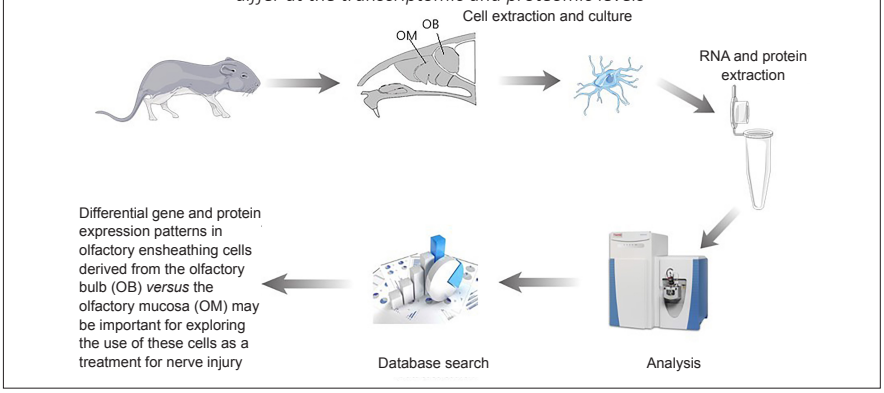

Abstract

Olfactory ensheathing cells (OECs) from the olfactory bulb (OB) and the olfactory mucosa (OM) have the capacity to repair nerve injury. However, the difference in the therapeutic effect between OB-derived OECs and OM-derived OECs remains unclear. In this study, we extracted OECs from OB and OM and compared the gene and protein expression profiles of the cells using transcriptomics and non-quantitative proteomics techniques. The results revealed that both OB-derived OECs and OM-derived OECs highly expressed genes and proteins that regulate cell growth, proliferation, apoptosis and vascular endothelial cell regeneration. The differentially expressed genes and proteins of OB-derived OECs play a key role in regulation of nerve regeneration and axon regeneration and extension, transmission of nerve impulses and response to axon injury. The differentially expressed genes and proteins of OM-derived OECs mainly participate in the positive regulation of inflammatory response, defense response, cytokine binding, cell migration and wound healing. These findings suggest that differentially expressed genes and proteins may explain why OB-derived OECs and OM-derived OECs exhibit different therapeutic roles. This study was approved by the Animal Ethics Committee of the General Hospital of Ningxia Medical University (approval No. 2017-073) on February 13, 2017.
Key Words: biological process; cellular component; gene; Gene Ontology; Kyoto Encyclopedia of Genes and Genomes; molecular function; olfactory bulb; olfactory ensheathing cells; olfactory mucosa; protein

Chinese Library Classification No. R441; R338; R741.04

Introduction

Olfactory ensheathing cells (OECs) are a unique type of glial cell characterized by their lifelong nerve regeneration function. They secrete a variety of neurotrophic factors and neural adhesion molecules. OECs share similarities with Schwann cells and astrocytes (Barnett, 2004), and although OECs and Schwann cells are particularly similar, OECs have some unique characteristics. OECs exist in the peripheral nervous system (as with Schwann cells) and in the central nervous system (as with astroglia). The olfactory mucosa (OM) can regenerate throughout life, including in humans; however, the specific mechanism of regeneration, and how this process may involve OECs, are not yet clear. OECs stimulate axon growth and cell migration in a stronger manner than Schwann cells (Ramón-Cueto et al., 1998). Astrocytes have a beneficial effect on neuron survival and axon growth; transplanted OECs also wrap around neurons to form myelin sheaths that support the

[1]School of Clinical Medicine, Ningxia Medical University, Yinchuan, Ningxia Hui Autonomous Region, China; [2]Ningxia Human Stem Cell Institute, General Hospital of Ningxia Medical University, Yinchuan, Ningxia Hui Autonomous Region, China; [3]Department of Neurosurgery, General Hospital of Ningxia Medical University, Yinchuan, Ningxia Hui Autonomous Region, China; [4]Clinical Laboratory Center, General Hospital of Ningxia Medical University, Yinchuan, Ningxia Hui Autonomous Region, China; [5]School of International Education, Ningxia Medical University, Yinchuan, Ningxia Hui Autonomous Region, China; [6]Biochip Research Center, General Hospital of Ningxia Medical University, Yinchuan, Ningxia Hui Autonomous Region, China
*Correspondence to: He-Chun Xia, xhechun@nyfy.com.cn; Li-Bin Wang, PhD, wanglibin007@126.com.
https://orcid.org/0000-0002-9609-7809 (Yuan-Xiang Lan); https://orcid.org/0000-0002-7861-1560 (Li-Bin Wang);
https://orcid.org/0000-0002-3058-8162 (He-Chun Xia)
#Both authors contributed equally to the work.

Funding: *This work was supported by Key Research Projects of Ningxia Hui Autonomous Region of China, No. 2018BCG01002 (to HCX) and the Natural Science Foundation of Ningxia Hui Autonomous Region of China, No. NZ17150 (to PY).*
How to cite this article: *Lan YX, Yang P, Zeng Z, Yadav N, Zhang LJ, Wang LB, Xia HC (2022) Gene and protein expression profiles of olfactory ensheathing cells from olfactory bulb versus olfactory mucosa. Neural Regen Res 17(2):440-449.*

growth of nerve processes after a nerve defect (Devon and Doucette, 1992; Gu et al., 2019). These characteristics make OECs one of the best choices for the treatment of neurological diseases and injury (Abdel-Rahman et al., 2018; Kim et al., 2018; Yao et al., 2018; Reshamnala et al., 2020; Yang et al., 2020; Wang et al., 2021).

OECs used in research are usually derived from the olfactory bulb (OB) (Franssen et al., 2007), although harvesting OECs from the OM is easier in clinical practice (Miedzybrodzki et al., 2006). Previous studies have shown that OB-derived OECs and OM-derived OECs have many similar and different functions (Richter et al., 2005; Bergström et al., 2007; Wang et al., 2014; Smith et al., 2020). Guérout et al. (2010) found relatively large differences in expression of many genes related to wound repair and nerve regeneration in the two cell types. OECs from the OB and the OM can repair nerve injury (Gu et al., 2017). However, the difference in the therapeutic effect between OB-derived OECs and OM-derived OECs remains unclear. Therefore, we hypothesized that OB-derived and OM-derived OECs will differ in protein expression levels. In this study, we used current, well-established transcriptomic and proteomic techniques to explore differences between OECs from OB and OM. We explain why OECs from OB and OM have different therapeutic effects, which should provide a new theoretical basis for future clinical treatments.

Materials and Methods

Isolation of OECs by cell culture

This study was approved by the Animal Ethics Committee of the General Hospital of Ningxia Medical University (approval No. 2017-073) on February 13, 2017. All experimental procedures described here were in accordance with the National Institutes of Health Guidelines for the Care and Use of Laboratory Animals (National Institutes of Health Publication No. 85-23, revised 1996). The experimental animals were subjected to all operations under anesthesia, and every effort was made to minimize their pain and suffering.

Ten 1-week-old Institute of Cancer Research (ICR) mice, weighing 7 ± 0.5 g, were provided by the Animal Experiment Center of Ningxia Medical University, license No. SCXK (Ning) 2015-0001. The mice were deeply anesthetized by 5% isoflurane (Cat# 217190101, RWD, Shenzhen, China) inhalation and were then decapitated. The skull was peeled off quickly from the foramen magnum of the head of the mouse to fully expose the medulla oblongata, cerebellum, cerebrum and OB to ensure the integrity of the OB. The OB on the posterior side of the nasal septum and the OM on the epithelial surface were quickly separated and placed in cooled phosphate buffered saline (PBS; Cat# 8120062, Thermo Fisher Biochemical Product (Beijing) Co. Ltd., Beijing, China) on ice. The OB and OM surfaces were gently washed three times to remove excess blood. Each tissue type was cut carefully with ophthalmic scissors, ground with a micropipette and placed into a tube. The OB and OM samples were incubated at 37°C for 20 minutes with 0.1% trypsin (Cat# 12604021, Thermo Fisher Scientific, Grand Island, NY, USA). After addition of culture medium consisting of Dulbecco's modified Eagle medium/nutrient mixture F12 medium (Cat# 2186850, Thermo Fisher Scientific), 10% fetal bovine serum (Cat# 1048791, Biological Industries Israel, Kibbutz Beit-Haemek, Israel) and 1% penicillin-streptomycin liquid (Cat# P1400, Solarbio, Beijing, China), the OB and OM samples were centrifuged at 800 × *g* for 5 minutes, the pellet was resuspended in fresh culture medium and the samples were centrifuged again at 800 × *g* for 5 minutes. After removal of the supernatant, the samples were again resuspended in culture medium and filtered with a 200-μm mesh filter to obtain uniform cell suspensions. The cells were seeded in six-well plates (Cat# 031819AA01, Wuxi NEST Biotechnology Co., Ltd., Wuxi, China) at 1×10^6 cells/mL/well, and the six-well plates were incubated at 37°C and 5% CO_2. After 18 hours of incubation, the cell suspensions were centrifuged at 800 × *g* for 5 minutes, the pellets were resuspended in fresh culture medium and incubated in new six-well plates for 24 hours. The cell suspensions were centrifuged again at 800 × *g* for 5 minutes, then seeded in six-well plates coated with poly-L-lysine (Cat# RNBD4661, Sigma-Aldrich, St. Louis, MO, USA) for 48 hours of incubation. The cells were separated by the modified Nash differential adhesion method (Peng et al., 2009), and finally, purified OB and OM cells were obtained, as previously described (Choi et al., 2008; Wang et al., 2014; Yao et al., 2018). The culture medium for the primary cells was refreshed every 2 days. When cells reached 80% confluence, they were collected for future experiments.

Identification and Purification of OECs

On day 1, OB and OM cells grown on slides (Cat# 10210008CE, CITOTEST, Haimen, China) were washed three times with PBS for 3 minutes each time, fixed with 4% paraformaldehyde for 15 minutes and rinsed three times with PBS for 3 minutes each time. The cells were permeated with 0.5% Triton X-100 in PBS (T8200, Solarbio) for 20 minutes at room temperature, and the slides were immersed in PBS three times for 5 minutes each time. The PBS was removed using absorbent paper, and the slides were treated with 5% bovine serum albumin blocking solution (SW3015, Solarbio) at room temperature for 30 minutes. After removal of blocking solution with absorbent paper, without washing, the slides were treated with the primary antibodies neurotrophin receptor 2% P75 in PBS (rabbit, 1:50, Cat# ab52987, Abcam, Cambridge, UK) and 1% S100 in PBS (rabbit, 1:100, Cat# ab52642, Abcam) and incubated overnight at 4°C in a humid box. On day 2, the slides were soaked in PBS three times for 3 minutes each time. After removal of excess liquid, the slides were treated with the diluted fluorescent cross-absorbed secondary antibodies Alexa Fluor 594 (goat anti-rabbit, 1:200, Cat# A-21203, Invitrogen, Eugene, OR, USA) and Alexa Fluor 488 (goat anti-rabbit, 1:200, Cat# A-21202, Invitrogen) in the dark at 37°C for 1 hour, then washed with PBS three times for 3 minutes each time. After 4′,6-diamidino-2-phenylindole (DAPI; Cat# D9542, Sigma-Aldrich) was added dropwise, slides were incubated in the dark for 5 minutes to stain the cells. PBS was used to wash away excess DAPI. After removing the liquid with absorbent paper, the slides were sealed with antifading mounting medium (Cat# 20181130, Solarbio) and observed under a fluorescence microscope (IJ21181; Olympus, Tokyo, Japan). Five fields of view were randomly selected under the microscope to count cells. The total number of nuclei was counted. The number of P75- or S100-positive cells and the number of cells with nuclei co-stained with DAPI were counted. Purity of OECs (%) = (P75-positive + DAPI-positive cells, or S100-positive + DAPI-positive cells)/DAPI-positive cells × 100.

RNA preparation

For RNA samples, the culture medium was removed when cells were at 80% confluence, and cells were lysed in an appropriate amount of TRIzol™ reagent (Cat# 15596026, Thermo Fisher Scientific) and stored in 1.5 mL RNase-free tubes at –80°C. For protein samples, cells at passage 3–5 were washed with cold PBS three times, scraped into centrifuge tubes and centrifuged at 800 × *g* at 4°C for 5 minutes. After supernatant removal, each tube opening was sealed with a sealing membrane, and the tubes were stored at –80°C.

RNA quality determination

RNA purity was determined using a K5500® spectrophotometer (Kaiao, Beijing, China). RNA integrity and concentration were assessed using the RNA Nano 6000 Assay Kit (Agilent Technologies, Santa Clara, CA, USA) and the Bioanalyzer 2100 system (Agilent Technologies).

Library preparation for RNA sequencing
RNA sequencing samples were prepared using 2 μg RNA per sample. Sequencing libraries were generated using NEBNext® Ultra™ RNA Library Prep Kit for Illumina® (Cat# E7530L, New England BioLabs, Inc., Ipswich, MA, USA) in accordance with the manufacturer's instructions, and index codes were added to attribute sequences to each sample.

Library examination
RNA concentration of the library was measured using the Qubit® RNA Assay Kit (Thermo Fisher, Waltham, MA, USA) in Qubit® 3.0 and then diluted to 1 ng/μL. Insert size was assessed using the Agilent Bioanalyzer 2100 system, and qualified insert size was accurately quantified using the StepOnePlus™ Real-Time polymerase chain reaction system (Thermo Fisher Scientific) (library valid concentration > 10 nM).

Library clustering and sequencing
The clustering of the index-coded samples was performed on a cBot cluster generation system (Illumina, San Diego, CA, USA) using a HiSeq PE Cluster Kit v4-cBot-HS (Illumina) in accordance with the manufacturer's instructions. After cluster generation, the libraries were sequenced on an Illumina platform, and 150 base pair paired-end reads were generated.

Protein preparation
Samples from passage 3 OECs were sonicated three times on ice using a high-intensity ultrasonic processor (Ningbo Scientz Biotechnology Co., Ltd., Ningbo, China) in lysis buffer (8 M urea [Sigma, Burlington, VT, USA] and 1% protease inhibitor cocktail [Sigma]). Remaining debris was removed by centrifugation at 12,000 × *g* at 4°C for 10 minutes. Finally, the supernatant was collected, and the protein concentration was determined with a bicinchoninic acid protein assay kit (Cat# P0012, Beyotime, Shanghai, China) in accordance with the manufacturer's instructions.

For digestion, the protein solution was reduced with 5 mM dithiothreitol for 30 minutes at 56°C and alkylated with 11 mM iodoacetamide for 15 minutes at room temperature in the dark. The protein samples were diluted by adding 100 mM triethylammonium bicarbonate (Sigma) to urea concentration < 2 M. Finally, trypsin (Yaxin Biotechnology Co., Ltd., Shanghai, China) was added at 1:50 trypsin-to-protein mass ratio for the first digestion overnight and at 1:100 trypsin-to-protein mass ratio for a 4-hour digestion.

Liquid chromatography-tandem mass spectrometry analysis
The peptides were dissolved in the mobile phase A of liquid chromatography (0.1% [v/v] formic acid [Fluka, Burlington, VT, USA] in water) and then separated using the nanoElute® ultra-high performance liquid system (Bruker Daltonics, Billerica, MA, USA). The peptides were injected into the capillary ion source for nanospray ionization and analyzed by time-of-flight tandem mass spectrometry (MS/MS) (Bruker Daltonics) using Q Exactive™ Plus (Thermo Fisher Scientific).

Database search
The resulting MS/MS data were processed using the MaxQuant search engine (v.1.6.6.0; http://www.coxdocs.org/doku.php?id=maxquant:start). Tandem mass spectra were searched against the human UniProt database concatenated with a reverse decoy database. Carbamidomethylation of cysteine was specified as a fixed modification, and acetylation modification and oxidation on methionine were specified as variable modifications (Cox and Mann, 2008).

Gene ontology annotation and enrichment analysis
Gene Ontology (GO) analysis (Ashburner et al., 2000; Thomas, 2017) is a bioinformatics analysis method that can organically link information from genes and gene products (such as proteins) to provide statistical information. The GO annotation proteome was derived from the UniProt-GOA database (http://www.ebi.ac.uk/GOA/). First, identified protein IDs were converted to UniProt IDs and then mapped to GO IDs. If identified proteins were not annotated by the UniProt-GOA database, the InterProScan software was used to annotate the protein's GO function based on the protein sequence alignment method. Second, proteins were classified by GO annotation based on three categories: "biological process," "cellular component," and "molecular function." For each category, a two-tailed Fisher's exact test was employed to test the enrichment of a differentially expressed protein against all identified proteins. The GO with a corrected *P*-value < 0.05 was considered significant.

Kyoto encyclopedia of genes and genomes pathway annotation and enrichment analysis
The Kyoto Encyclopedia of Genes and Genomes (KEGG) (Ogata et al., 1999; Chen et al., 2020a) combines current protein interaction network information, such as pathways and related complexes ("pathway" database), genes and gene products ("gene" database) and biological complexes and relevant reactions ("compound and reaction" database). KEGG's pathways include metabolism, genetic-information processing, environmental information-related processes, cellular physiological processes and drug research (Du et al., 2014). We used the KEGG pathway database to annotate protein pathways: first, using the KEGG online service tool KAAS (v. 2.0; http://www.genome.jp/kaas-bin/kaas_main) to annotate the submitted proteins, then using the KEGG mapper to match the annotated proteins to corresponding pathways in the database.

Parallel reaction monitoring data analysis
The resulting MS data were processed using Skyline (v. 3.6; https://skyline.ms/project/home/software/Skyline/begin.view). For the peptide settings, enzyme was set as trypsin (KR/P) and maximum missed cleavage was set to 0. The peptide length was set as 7–25 amino acids, fixed modification was set as carbamidomethylation on cysteine, and maximum variable modifications was set to 3. For the transition settings, precursor charges were set to 2, 3; ion charges were set to 1, 2; and ion types were set to b, y, p. The product ions were set from ion 3 to the last ion, and the ion match tolerance was set as 0.02 Da.

Data analysis
The hypergeometric test was used for functional enrichment analysis, and Fisher's exact test using R was used to calculate *P* values. The R package DESeq2 (http://www.bioconductor.org/packages/DESeq2/ (Love et al., 2014)) was used to analyze differentially expressed genes. The hierarchical cluster method was used to generate the expression heat map. All *P* values were adjusted using the Benjamini-Hochberg procedure to decrease the false discovery rate. All calculation steps were performed in RStudio (https://rstudio.com/products/rstudio/download/#download).

Results

Identification of OECs from OB and OM
We purified OECs using a modified Nash differential adhesion method. In the *in vitro* culture environment, most of the suspended cells adhered to the six-well plates' walls at 36 hours. Two main types of cells were identified morphologically. In the OB samples, almost all cells were bipolar or tripolar. In the OM samples, some cells were flat and polygonal with darkened cell bodies and several pseudopod-like structures, and were possibly early fibroblasts; other cells were bipolar or tripolar. However, it was difficult to accurately distinguish cell types at this 36-hour time point. Three days later, the differences between the two cell morphologies were more apparent. We identified fibroblasts, which had irregular

shapes, a poor refractive index and divided rapidly, and OECs, which had clear outlines, strong three-dimensionality and bipolar or tripolar protrusions. OECs from the OB were dominated by bipolar cells with symmetrical protrusions. The cell body was long and spindle-shaped, and the nucleus was in the center. OECs from the OM were dominated by tripolar cells with three protrusions. The purification rate of both samples of cells was relatively high (85.4 ± 3.7%) after immunofluorescence identification with P75 and S100 (Lazzari et al., 2016; Śmieszek et al., 2017; Lin et al., 2019; Yue et al., 2020). There was no obvious difference in the expression level of P75 and S100 between cells from OB and OM, indicating that cells were separated and cultured successfully (**Figure 1**).

Differentially expressed genes and proteins in OB-derived and OM-derived OECs

This study detected 878 genes that were significantly differentially expressed in OB-derived OECs compared with OM-derived OECs, of which 419 were upregulated and 459 were downregulated. Cluster analysis was used to reflect changes in the pattern of differentially expressed genes in samples under different experimental conditions.

We used DESeq2 for differential gene expression analysis of OB-derived and OM-derived OECs. We calculated the Euclidean distance based on the expression level [fragments per kilobase of exon per million fragments mapped (FPKM)] of the differentially expressed genes in each sample and took the logarithm to the base 2. We then used the hierarchical cluster method to determine the overall clustering results of the samples. A heat map of all differentially expressed genes was generated (**Figure 2A**).

In this study, we used mass spectrometry to detect the signal abundance of proteins in each sample and obtained the label-free quantification (LFQ) intensity of these proteins using a non-standard quantitative calculation method. The relative quantification of each sample was determined by comparing the protein LFQ intensity values of the samples. We quantified 266 differentially expressed proteins in OB-derived OECs and OM-derived OECs, of which 236 were increased and 30 were decreased in OM-derived OECs compared with OB-derived OECs. We generated a quantitative volcano map of the differentially expressed proteins (**Figure 2B**). GO analysis of OECs from OB and OM showed that the most significant differences in genes, in terms of "molecular function," related to "glial cell–derived neurotrophic factor receptor binding," "neuregulin receptor activity" and "death receptor activity." The most significant differentially expressed protein in OB-derived OECs was related to "hydro-lyase activity"; in OM-derived OECs, it was related to "structural constituent of ribosome." In terms of "cellular component," the most significant differences in genes related to "clathrin-sculpted gamma-aminobutyric acid transport vesicle membrane," "semaphorin receptor complex" and "perisynaptic extracellular matrix." The proteins with significant differences in OB-derived OECs were related to "mitochondrion"; OM-derived OECs were related to "cytosolic ribosome." In terms of "biological process," the difference in genes related to "sclerotome development" was the most significant. The proteins with significant differences in OB-derived OECs were related to "aerobic respiration"; OM-derived OECs were related to "amide biosynthetic process" (**Figures 3** and **4**).

Through analysis and testing, we found that in OECs from OB and OM, the most significantly expressed genes and proteins involve "regulation of reproductive process" (GO:2000241), "cell adhesion" (GO:0007155), "regulation of cell migration" (GO:0030334), "positive regulation of developmental process" (GO:0051094), "regulation of nervous system development" (GO:0051960), "axon guidance" (GO:0007411), "regulation of neurogenesis" (GO:0050767), "regulation of axonogenesis" (GO:0050770), "protein dimerization activity" (GO:0046983), "protein homodimerization activity" (GO:0042803), "death receptor activity" (GO:0005035), "cytokine binding" (GO:0019955), "growth factor binding" (GO:0019838), "cell adhesion molecule binding" (GO:0050839), "neurotrophin binding" (GO:0043121), "transporter activity" (GO:0005215), "cytokine activity" (GO:0005125), "transforming growth factor beta receptor binding" (GO:0005160), "growth factor activity" (GO:0008083), "neurotrophin receptor activity" (GO:0005030) and "nerve growth factor binding" (GO:0048406) (**Table 1**).

To thoroughly understand the genes and proteins identified and quantified in our data, we elaborated on the functions and characteristics of these genes and proteins in terms of GO and the KEGG pathway. We obtained the enrichment results of differentially expressed genes in the secondary GO entries. At the same time, we plotted the functional classification of significantly enriched differentially expressed proteins ($P < 0.05$) (**Figures 3–5**; **Tables 2** and **3**). In terms of "molecular function," we found that two genes were highly expressed in OB-derived OECs compared with OM-derived OECs in the "glial cell-derived neurotrophic factor receptor binding" category of GO analysis. For the "death receptor activity" category, one gene was highly expressed in OB-derived OECs, and three genes were highly expressed in OM-derived OECs. Compared with OM-derived OECs, three proteins related to "hydro-lyase activity" were expressed at higher levels in OB-derived OECs; 33 proteins related to the "structural constituent of ribosome" were expressed at higher levels in OM-derived OECs. In terms of "cellular component," two genes were highly expressed in OB-derived OECs under the "clathrin-sculpted gamma-aminobutyric acid transport vesicle membrane" category of GO analysis. Fifteen proteins related to "mitochondrion" were expressed at higher levels in OB-derived OECs; 35 proteins related to "cytosolic ribosome" were overexpressed in OM-derived OECs. In terms of "biological process," the differentially expressed genes related to "sclerotome development" were most significantly enriched. Four genes were highly expressed in OM-derived OECs. Five proteins related to "aerobic respiration" were highly expressed in OB-derived OECs. Forty-nine proteins related to "amide biosynthetic process" were highly expressed in OM-derived OECs.

The hypergeometric test was applied to enrichment analysis for each pathway in KEGG, and the pathways that were significantly enriched in differentially expressed genes were identified. The extraction and union of the enrichment pathways of the comparison group were combined, and the KEGG entry was analyzed according to the enrichment degree q value of the sample in the pathway (**Figure 5A**). For the differentially expressed proteins identified by proteomics, the functional classifications and pathways of the significantly enriched proteins were determined by $P < 0.05$ (obtained by the enrichment test; Fisher's exact test) (**Figure 5B**). In this study, there were five KEGG pathways with the highest enrichment, namely "cytokine-cytokine receptor interaction," "cell adhesion molecules (CAMs)," "axon guidance," "malaria" and "Rap1 signaling pathway." Our data show that OM-derived OECs had 22 genes related to the "cytokine-cytokine receptor interaction" pathway, whereas OB-derived OECs had a greater number of differentially expressed genes in the "cell adhesion molecules (CAMs)" and "axon guidance" pathways (**Table 4**). Our proteomics sequencing shows that OB-derived OECs had five differentially expressed proteins enriched in the "citrate cycle (TCA cycle)" pathway. In OM-derived OECs, 30 proteins were enriched in the "ribosome" pathway, 11 proteins were enriched in the "tight junction" pathway and 7 significant proteins were enriched in the "adherens junction" pathway.

We conducted parallel reaction monitoring verification on *Atp6v1a*, *Cfl1*, *Dpysl2* and *Ywhae* of most interest, obtained relevant data for analysis, confirming that these four proteins were indeed highly expressed in OECs, further confirming the results of our protein screening (**Table 5**).

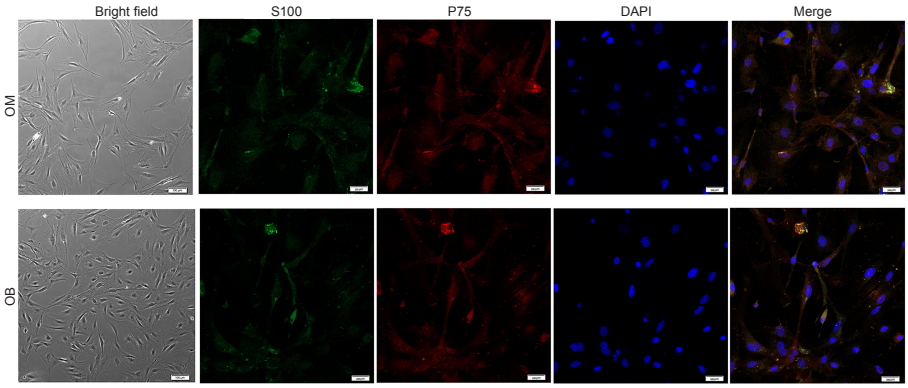

Figure 1 | Identification of olfactory ensheathing cells from the OM and OB.
Olfactory ensheathing cells from the OM and OB are dominated by tripolar cells with three protrusions and bipolar cells with symmetrical protrusions, respectively. The cell body is long and spindle-shaped, and the nucleus is in the center. Both cell types have slender protrusions in common. Olfactory ensheathing cells from the OM and OB express P75 (red, stained by Alexa Fluor 594) and S100 (green, stained by Alexa Fluor 488). Scale bars: 100 μm in the left column, 200 μm in the other columns. DAPI: 4′6-Diamidino-2-phenylindole; OB: olfactory bulb; OM: olfactory mucosa; P75: neurotrophin receptor P75.

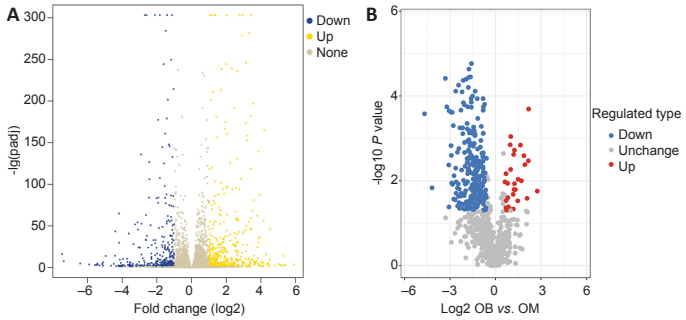

Figure 2 | Quantitative volcano map of differentially expressed genes (A) and proteins (B) of olfactory ensheathing cells from olfactory bulb compared with olfactory mucosa.
The *x*-axis is the expression multiple change, the *y*-axis is the statistical significance of the expression change; different colors indicate different classifications. For OB compared with OM, blue represents down-regulated genes or proteins, yellow and red represent up-regulated genes or proteins, and gray represents genes or proteins with no significant difference in expression. OB: Olfactory bulb; OM: olfactory mucosa; padj: *P*-value adjusted.

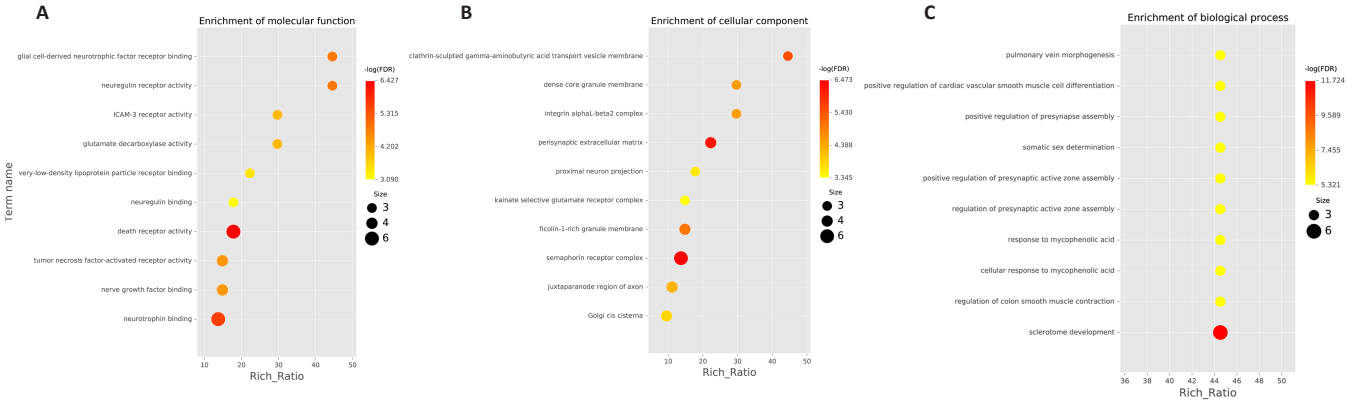

Figure 3 | Bubble chart of "molecular function" (A), "cellular component" (B) and "biological process" (C) of differentially expressed genes in olfactory ensheathing cells from olfactory bulb and olfactory mucosa.
The vertical axis of the bubble chart is the function label of the Gene Ontology item, and the horizontal axis value is the enrichment ratio of the differentially expressed genes. The differentially expressed genes related to "glial cell-derived neurotrophic factor receptor binding," "clathrin-sculpted gamma-aminobutyric acid transport vesicle membrane" and "sclerotome development" were most obviously enriched.

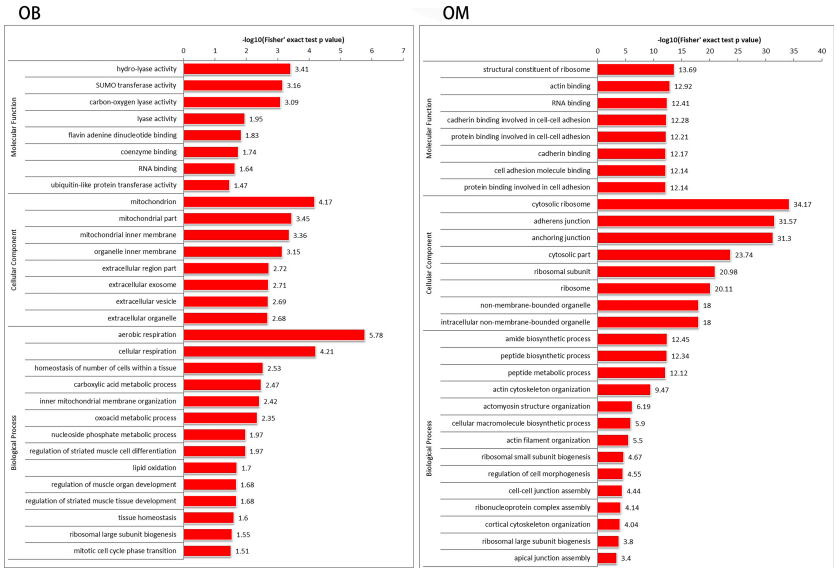

Figure 4 | Functions of OB and OM differentially expressed proteins in GO.
The enrichment distribution bar graph is separated by classification. The *y*-axis describes the GO terms; the *x*-axis is the *P*-value of Fisher's exact test. The most overexpressed proteins of OB are related to "hydro-lyase activity," "mitochondrion" and "aerobic respiration"; the most overexpressed proteins of OM are related to "structural constituent of ribosome," "cytosolic ribosome" and "amide biosynthetic process." GO: Gene ontology analysis; OB: olfactory ensheathing cells derived from the olfactory bulb; OM: olfactory ensheathing cells derived from the olfactory mucosa.

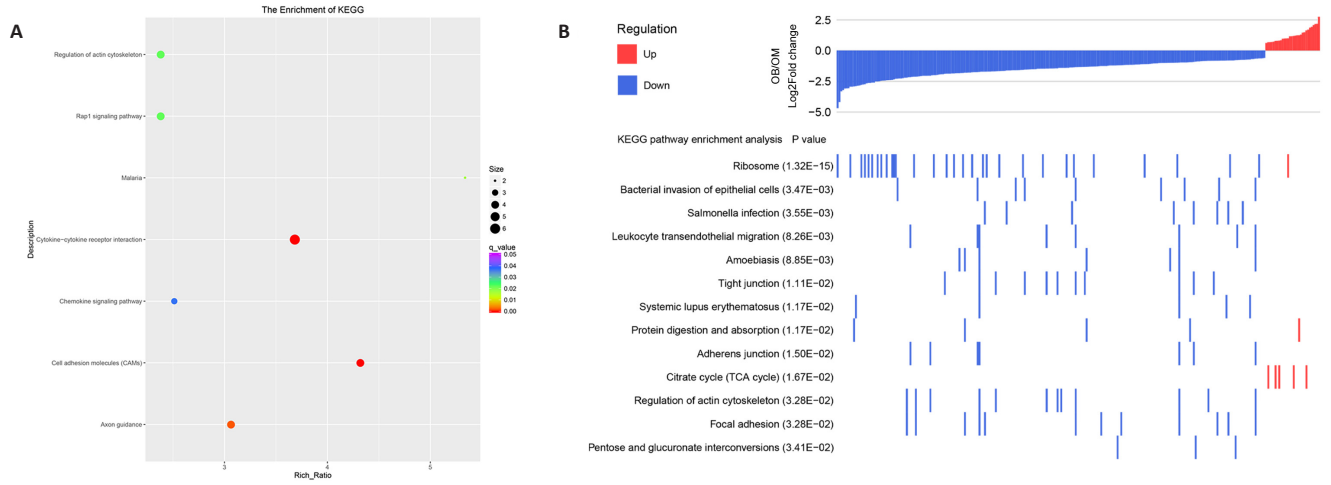

Figure 5 | The KEGG pathway for the significant enrichment of overexpressed genes (A) and proteins (B).
(A) Bubble diagram of the enrichment and distribution of overexpressed genes in the KEGG pathway. The x-axis is the enrichment factor of the differentially expressed genes and the y-axis is the name of the KEGG pathway. (B) Chart of the enrichment distribution of differentially expressed proteins in the KEGG pathway. Overexpressed genes are significantly enriched in KEGG pathways such as "cytokine-cytokine receptor interaction," "cell adhesion molecules" and "axon guidance" pathways. OB overexpressed proteins in the "citrate cycle (tricarboxylic acid cycle)" pathway; OM overexpressed proteins in the "ribosome" and "tight junction" pathways. Different colors indicate q value of enrichment. Circle size indicates number of differentially expressed genes. KEGG: Kyoto Encyclopedia of Genes and Genomes analysis; OB: olfactory ensheathing cells derived from the olfactory bulb; OM: olfactory ensheathing cells derived from the olfactory mucosa.

Table 1 | GO iterms with significantly enriched differentially expressed genes of OB and OM

Accession	Term_name	*P*-value	False discovery rate	Rich_ Ratio
GO:2000241	Regulation of reproductive process	0.004183	0.026152	2.439715
GO:0007155	Cell adhesion	9.88E-21	3.06E-18	3.070676
GO:0030334	Regulation of cell migration	1.87E-22	8.65E-20	3.129862
GO:0051094	Positive regulation of developmental process	2.94E-21	1.01E-18	2.47251
GO:0051960	Regulation of nervous system development	4.65E-19	1.04E-16	2.661375
GO:0007411	Axon guidance	7.35E-14	7.84E-12	5.407871
GO:0050767	Regulation of neurogenesis	1.13E-15	1.75E-13	2.544275
GO:0050770	Regulation of axonogenesis	6.09E-06	0.00013	3.191742
GO:0046983	Protein dimerization activity	2.55E-06	0.00016	1.615682
GO:0042803	Protein homodimerization activity	0.000132	0.00325	1.633201
GO:0005035	Death receptor activity	4.76E-05	0.001617	17.80992
GO:0019955	Cytokine binding	3.40E-05	0.001331	3.884714
GO:0019838	Growth factor binding	1.69E-06	0.000125	3.615262
GO:0050839	Cell adhesion molecule binding	5.17E-11	3.25E-08	3.675397
GO:0043121	Neurotrophin binding	0.000154	0.003712	13.69994
GO:0005215	Transporter activity	0.000293	0.005107	1.584605
GO:0005125	Cytokine activity	5.85E-05	0.001934	2.648784
GO:0005160	Transforming growth factor beta receptor binding	0.00225	0.02571	4.45248
GO:0008083	Growth factor activity	6.32E-07	5.67E-05	4.252369
GO:0048406	Nerve growth factor binding	0.000857	0.011579	14.8416

GO: Gene ontology; OB: olfactory ensheathing cells derived from the olfactory bulb; OM: olfactory ensheathing cells derived from the olfactory mucosa.

Table 2 | Distribution of OB and OM differentially expressed genes in GO enrichment analysis

GO terms level 1	Term name	GO terms ID	Gene count		
			OB	OM	Total
Molecular function	Glial cell-derived neurotrophic factor receptor binding	GO:0030116	2	0	2
	Neuregulin receptor activity	GO:0038131	1	1	2
	Death receptor activity	GO:0005035	1	3	4
	Neurotrophin binding	GO:0043121	3	1	4
Cellular component	Clathrin-sculpted gamma-aminobutyric acid transport vesicle membrane	GO:0061202	2	0	2
	Semaphorin receptor complex	GO:0031224	3	1	4
	Perisynaptic extracellular matrix	GO:0016021	2	1	3
Biological process	Sclerotome development	GO:0061056	0	4	4

GO: Gene ontology; OB: olfactory ensheathing cells derived from the olfactory bulb; OM: olfactory ensheathing cells derived from the olfactory mucosa; Terms level 1: the first-level classification item of GO enrichment analysis.

Table 3 | The quantitative distribution of OB and OM differentially expressed proteins in GO enrichment analysis

GO terms level 1	GO terms description	GO terms ID	Mapping	Regulated cell type
Molecular function	Hydro-lyase activity	GO:0016836	3	OB
	Structural constituent of ribosome	GO:0003735	33	OM
Cellular component	Mitochondrion	GO:0005739	15	OB
	Cytosolic ribosome	GO:0022626	35	OM
Biological process	Aerobic respiration	GO:0009060	5	OB
	Amide biosynthetic process	GO:0043604	49	OM

GO: Gene ontology; OB: olfactory ensheathing cells derived from the olfactory bulb; OM: olfactory ensheathing cells derived from the olfactory mucosa; Terms level 1: the first-level classification item of GO enrichment analysis.

Table 4 | **Quantitative enrichment analysis of differentially expressed genes of OB compared with OM in KEGG signaling pathway**

Name	KEGG map	*P*-value	q-value	Up_Gene*	Down_Gene*
Cytokine-cytokine receptor interaction	map04060	1.14E-09	3.94E-07	Cd40|K03160; Tnfsf15|K05478; Cxcl2|K05505; Tnfrsf19|K05155; Tnfsf18|K05479	Ccl3|K05408; Ccl6|K05510; Ccl4|K12964; Ccl9|K22671; Ccl11|K16597; Tgfb3|K13377; Bmp4|K04662; Tnfrsf25|K05160; Il18rap|K05174; Il1rl1|K05171; Tnfrsf11a|K05147; Il1rn|K05481; Il1b|K04519; Tnfrsf9|K05146; Cxcl9|K05416; Il13ra2|K05077; Ccl17|K21083; Gdf7|K20013; Il31ra|K22630; Gdf6|K20012; Csf2rb|K04738; Gm16008|K05154
Cell adhesion molecules	map04514	1.53E-07	2.64E-05	Cadm3|K06780; Cd40|K03160; Nrcam|K06756; Nfasc|K06757; Itga6|K06485; L1cam|K06550; Cadm1|K06781; Nrxn2|K07377; Cntnap2|K07380; Ntng1|K07522; Nlgn1|K07378	Itgb2|K06464; Cldn1|K06087; Nrxn1|K07377; Ptprc|K06478; Selp|K06496; Siglec1|K06548
Axon guidance	map04360	1.75E-05	0.002023	Sema4f|K06521; Sema6b|K06842; Sema3g|K06840; Sema4c|K06521; Nfatc2|K17332; Epha5|K05106; Plxna4|K06820; Plxnb3|K06821; L1cam|K06550; Wnt4|K00408; Sema7a|K06529; Ntng1|K07522	Shh|K11988; Rac2|K07860; Sema3f|K06840; Gdf7|K20013; Plxnc1|K06572
Malaria	map05144	0.000201	0.017389	Cd40|K03160	Itgb2|K06464; Cd36|K06259; Tgfb3|K13377; Selp|K06496; Il1b|K04519; Hgf|K05460
Rhoptry-associated protein 1 signaling pathway	map04015	0.000385	0.022218	Pdgfb|K17386; Kit|K05091; Fyb|K17698; Adcy5|K08045; Arap3|K12490; Fgf5|K04358; Gm8399|K05692; Cnr1|K04277; Fgf18|K04358	Itgb2|K06464; Rapgef3|K08014; Hgf|K05460; Pdgfra|K04363; Vegfd|K05449; Rac2|K07860; Rapgef5|K08019; Fpr1|K04172

* Gene name|protein accession number. KEGG: Kyoto Encyclopedia of Genes and Genomes analysis; OB: olfactory ensheathing cells derived from the olfactory bulb; OM: olfactory ensheathing cells derived from the olfactory mucosa.

Table 5 | **Parallel Reaction Monitoring quantitative analysis results from the unique peptide of the selected protein**

Protein accession	Gene	OB/OE ratio	OB/OE ratio (LQ)	OB/OE *P*-value	Peptide	Retention time (min)
P50516	*Atp6v1a*	1.76	3.66	8.15E-03	GVNVSALSR	13.22
					WEFIPSK	19.32
P18760	*Cfl1*	0.77	0.56	3.61E-01	EILVGDVGQTVDDPYTTFVK	23.58
					HELQANCYEEVK	10.85
O08553	*Dpysl2*	0.66	0.57	2.30E-03	SITIANQTNCPLYVTK	18.41
					GSPLVVISQGK	17.39
P62259	*Ywhae*	0.35	0.64	3.37E-02	IISSIEQK	11.32
					EAAENSLVAYK	13.68

In the experimental design, more than two unique peptides for quantification were used for each protein. Atp6v1a: ATPase H^+ transporting V1 subunit A; Cfl1: Cofilin-1; Dpysl2: dihydropyrimidinase-like 2; LQ: label-free quantity; OB: olfactory ensheathing cells derived from the olfactory bulb; OM: olfactory ensheathing cells derived from the olfactory mucosa; Ywhae: 14-3-3 protein epsilon.

Discussion

We identified many highly expressed genes and proteins in OB and OM using GO analysis. For example, OB overexpresses nerve growth factor receptor (Ngfr), which plays a key role in apoptosis, nerve growth factor binding, axon guidance, central nervous system development, nerve development and positive regulation of apoptotic processes (Ramli et al., 2019; Chen et al., 2020b; Sanders et al., 2020). Neurotrophic receptor tyrosine kinase 2 (Ntrk2), overexpressed by OB, can regulate central nervous system neuron development, positive regulation of axonogenesis, cell proliferation and neuron projection development (Chen et al., 2019; Badurek et al., 2020; Pattwell et al., 2020). There is evidence that Ntrk2 plays a protective role in prodromal Huntington's disease (Ciarochi et al., 2018). Insulin-like growth factor binding protein 3 (Igfbp3), overexpressed by OB, is related to positive regulation of apoptotic processes and regulation of cell growth (Arab et al., 2020; Tan et al., 2020). Semenova et al. (2020) found that Igfbp3 plays a significant role in propagation of stress-induced senescence in human endometrium-derived mesenchymal stem cells. Igfbp3 is a multifunctional protein that can stimulate cell growth or promote apoptosis. Kinase insert domain receptor (Kdr), overexpressed by OB, is related to blood-vessel endothelial-cell differentiation and cell migration, positive regulation of angiogenesis, cell migration, cell proliferation, focal adhesion assembly and positive regulation of vasculogenesis (Borowczyk et al., 2019; Li et al., 2019; Dono et al., 2020). These genes and proteins are highly expressed in OB, and the function of these genes explains why transplantation of OB-derived OECs after nerve damage can help animals or humans restore part of their nerve function (Voronova et al., 2019; Li et al., 2020) and demonstrates the important potential of OECs as a candidate for the treatment of nerve damage.

OM overexpresses sonic hedgehog, which is involved in spinal-cord motor-neuron differentiation, stem cell development, vasculogenesis, cell development, cell proliferation and other related processes (Yuan et al., 2019; Gredler et al., 2020; Hamdi-Rozé et al., 2020). Previous studies have shown that sonic hedgehog plays essential roles in developmental events such as cell-fate specification and axon guidance (Yam et al., 2009). Lowry et al. (2008) reported that transplantation of endothelial-expanded neural stem cells that were treated with sonic hedgehog during the expansion phase into an adult mouse SCI model resulted in significant recovery of sensory and motor function.

OM overexpresses bone morphogenetic protein 4 (Bmp4). Bmp4 plays an important role in angiogenesis, endothelial cell migration and blood vessel development and is a positive regulator of apoptotic processes, cell migration and the vascular endothelial growth factor-receptor signaling pathway (Peng et al., 2019; Kobayashi et al., 2020). This suggests that OM cells can promote the development of endothelial cells; wound healing is accompanied by the development of new endothelial-lined blood vessels. Taha et al. (2016)

demonstrated that Bmp4 signaling and serum composition play significant roles in the differentiation of mouse embryonic stem cells towards the endodermal lineage.

OM overexpresses tumor necrosis factor receptor superfamily member 25 (Tnfrsf25). Tnfrsf25 participates in the inflammatory response, regulation of apoptotic processes and regulation of cell proliferation. A previous study demonstrated that a two-pathway *in vivo* strategy targeting Tnfrsf25 [with tumor necrosis factor superfamily cytokine TNF-like protein 1A (TL1A-Ig)] and interleukin-2 receptor (with low-dose interleukin-2) can elicit strong increases in regulatory T cell numbers and functions (Copsel et al., 2020). This means that OM can enhance the body's immune response to fight against inflammation caused by nerve damage.

Other growth factors were also overexpressed. Transforming growth factor beta 3 (Tgfb3) is closely related to the activation of mitogen-activated protein kinase activity, cell development, cell growth, wound healing and positive regulation of apoptotic processes (Sarper et al., 2018; Galimberti et al., 2019; Meaburn and Misteli, 2019). Platelet-derived growth factor receptor alpha (Pdgfra) plays a key role in cell migration, platelet aggregation, positive regulation of cell migration, wound healing and positive regulation of cell proliferation (Urbini et al., 2019; Shi et al., 2020). The genes or proteins highly expressed by OM play an important role in the inflammatory response, blood vessel growth and wound repair. Recovery of wounds treated with OM-derived OECs has been shown to be faster compared with the OB-derived OECs comparison group (Li et al., 2020); therefore, OM-derived OECs are cells with great potential for use as a clinical treatment of nerve injury in the future.

By analyzing the data related to the KEGG pathway from OB-derived and OM-derived OECs, we found that the metabolic pathways identified from the two sources of cells are consistent with our GO enrichment analysis results. OM is enriched for differentially expressed proteins related to cytokine interaction, cell adhesion and tight junctions, such as C-C motif chemokine ligand 3 and C-C motif chemokine ligand 4. These proteins function as positive regulators of inflammatory response, cell migration and endothelial cell proliferation (Pelisch et al., 2020). Indraswari et al. (2009) found that the expression of dihydropyrimidinase-like 2 (Dpysl2) and cofilin-1 indicates an early neuronal defense mechanism leading to active neuronal repair, regeneration and development because these genes are involved in neurite outgrowth and plasticity. OB has an increased number of differentially expressed proteins related to axon growth and extension, such as neuronal cell adhesion molecule (Nrcam), which is related to neuron cell-cell adhesion and calcium-dependent cell-cell adhesion via plasma membrane cell adhesion molecules (Charoy et al., 2012). Neurofascin is related to axon guidance, protein localization to the paranode region of the axon, and transmission of nerve impulses (Thaxton et al., 2010; Monfrini et al., 2019). ATPase H^+ transporting V1 subunit A and 14-3-3 protein epsilon have been associated with epileptic encephalopathies (Kadwa, 2020; Romano et al., 2020). Collectively, through gene and protein analysis, this study shows that these highly expressed genes and proteins in OECs contribute to the inhibition of progressive tissue damage and functional impairment in nervous system disease.

The role of OECs is often underestimated, but as more studies reveal their promise in functional applications (Mackay-Sim and St John, 2011; Collins et al., 2019), it is necessary to better understand their gene and protein components and related functions. Compared with previous research on the difference between OB-derived and OM-derived OECs (Guérout et al., 2010; Alizadeh et al., 2019; Smith et al., 2020), our study identifies genes and proteins in mouse OB and OM based on MS analysis and analyzes the data by bioinformatics methods. In a previous study (Guérout et al., 2010), 57 overexpressed genes in OB and OM were identified; our study identified more than 800 overexpressed genes. We also detected significant differences in related proteins, providing more comprehensive data for future investigation.

Based on the genes and proteins we identified from OECs, we selected several proteins of interest for parallel reaction monitoring verification, *Atp6v1a*, *Cfl1*, *Dpysl2* and *Ywhae*. We confirmed that these proteins are indeed differentially expressed in OECs. *In vivo* experiments will be useful to perform in the future. Current research (Pastrana et al., 2006) shows that the expression of olfactory ensheathing cells *in vivo* and *in vitro* is not the same, which is closely related to their functional mechanism. For example, in the treatment of spinal cord injury, *in vitro*, OECs promote axonal growth as a source of neurotrophic growth factors; *in vivo*, they produce myelin, promoting remyelination of damaged axons (Pellitteri et al., 2014). We will explore the mechanisms of specific proteins of interest in OB-derived and OM-derived OECs *in vitro* in future research to understand the possible benefits for the treatment of neurological diseases and nerve injury after OEC transplantation.

In conclusion, OB expression is significantly related to aerobic respiration, cellular respiration and carboxylic acid metabolic processes. OB expression shows a stronger regulation of nerve regeneration and axon regeneration and extension processes, and these processes play key roles in transmission of nerve impulses and response to axon injury. Conversely, OM expression is significantly related to amide biosynthetic processes and peptide biosynthetic processes, and these processes play key roles in positive regulation of inflammatory response, positive regulation of defense response, cytokine binding, cell migration and regulation of wound healing. OECs from OB and OM overexpress genes and proteins involved in cell growth, proliferation and apoptosis, which are closely related to their role in treating nerve injury. The significantly differentially overexpressed genes and proteins identified herein may lead to further understanding of the different therapeutic effects of OB compared with OM for nerve injury. Therefore, our research will help to gain insights into the molecular activity of OECs, add further information to the relevant transcriptome and proteome maps, and could also aid in the discovery of biomarker proteins for diseases related to OECs in the future. Our research focused on the expression of OB-derived and OM-derived OECs *in vitro*, and failed to elaborate on the similarities, differences and mechanisms of expression *in vivo*. We believe that in the future, the systematic study of the gene and protein expression of olfactory ensheathing cells from two sources *in vivo* and *in vitro* will better explain the different reasons for their functions, and will greatly promote the clinical application of olfactory ensheathing cells.

Acknowledgments: *We thank Jingjie PTM BioLabs (Hangzhou, China) for supporting Label Free and parallel reaction monitoring proteomics analysis.*

Author contributions: *Design and concept of the study: YXL, PY, HCX, LBW; experiment conduction: YXL, PY, ZZ, LJZ; background analysis and manuscript preparation: YXL, HCX, LBW; manuscript editing: YXL, NY. All authors approved the final manuscript.*

Conflicts of interest: *The authors declare no conflicts of interest.*

Financial support: *This work was supported by Key Research Projects of the Ningxia Hui Autonomous Region of China, No. 2018BCG01002 (to HCX) and the Natural Science Foundation of Ningxia Hui Autonomous Region of China, No. NZ17150 (to PY). The funding sources had no role in study conception and design, data analysis or interpretation, paper writing or deciding to submit this paper for publication.*

Institutional review board statement: *This study was approved by the Animal Experiment Ethics Committee of the General Hospital of Ningxia Medical University (approval No. 2017-073) on February 13, 2017.*

Data sharing statement: *The original data including transcriptome and proteome are shown in iProX with ID proteome: PXD024046. RNA-seq data are openly available in GenBank of NCBI (https://www.ncbi.nlm.nih.gov/) under the accession. The associated BioProject, SRA, and BioSample numbers are SAMN17975094, SAMN17975093, PRJNA702555, respectively.*
Plagiarism check: *Checked twice by iThenticate.*
Peer review: *Externally peer reviewed.*

References

Abdel-Rahman M, Galhom RA, Nasr El-Din WA, Mohammed Ali MH, Abdel-Hamid AES (2018) Therapeutic efficacy of olfactory stem cells in rotenone induced Parkinsonism in adult male albino rats. Biomed Pharmacother 103:1178-1186.

Alizadeh R, Ramezanpour F, Mohammadi A, Eftekharzadeh M, Simorgh S, Kazemiha M, Moradi F (2019) Differentiation of human olfactory system-derived stem cells into dopaminergic neuron-like cells: A comparison between olfactory bulb and mucosa as two sources of stem cells. J Cell Biochem 120:19712-19720.

Arab JP, Cabrera D, Sehrawat TS, Jalan-Sakrikar N, Verma VK, Simonetto D, Cao S, Yaqoob U, Leon J, Freire M, Vargas JI, De Assuncao TM, Kwon JH, Guo Y, Kostallari E, Cai Q, Kisseleva T, Oh Y, Arrese M, Huebert RC, et al. (2020) Hepatic stellate cell activation promotes alcohol-induced steatohepatitis through Igfbp3 and SerpinA12. J Hepatol 73:149-160.

Ashburner M, Ball CA, Blake JA, Botstein D, Butler H, Cherry JM, Davis AP, Dolinski K, Dwight SS, Eppig JT, Harris MA, Hill DP, Issel-Tarver L, Kasarskis A, Lewis S, Matese JC, Richardson JE, Ringwald M, Rubin GM, Sherlock G (2000) Gene ontology: tool for the unification of biology. The Gene Ontology Consortium. Nat Genet 25:25-29.

Badurek S, Griguoli M, Asif-Malik A, Zonta B, Guo F, Middei S, Lagostena L, Jurado-Parras MT, Gillingwater TH, Gruart A, Delgado-García JM, Cherubini E, Minichiello L (2020) Immature dentate granule cells require Ntrk2/Trkb for the formation of functional hippocampal circuitry. iScience 23:101078.

Barnett SC (2004) Olfactory ensheathing cells: unique glial cell types? J Neurotrauma 21:375-382.

Borowczyk M, Szczepanek-Parulska E, Dębicki S, Budny B, Verburg FA, Filipowicz D, Wrotkowska E, Janicka-Jedyńska M, Więckowska B, Gil L, Ziemnicka K, Ruchała M (2019) Genetic heterogeneity of indeterminate thyroid nodules assessed preoperatively with next-generation sequencing reflects the diversity of the final histopathologic diagnosis. Pol Arch Intern Med 129:761-769.

Charoy C, Nawabi H, Reynaud F, Derrington E, Bozon M, Wright K, Falk J, Helmbacher F, Kindbeiter K, Castellani V (2012) gdnf activates midline repulsion by Semaphorin3B via NCAM during commissural axon guidance. Neuron 75:1051-1066.

Chen H, Zhang Y, Awasthi SK, Liu T, Zhang Z, Awasthi MK (2020a) Effect of red kaolin on the diversity of functional genes based on Kyoto Encyclopedia of Genes and Genomes pathways during chicken manure composting. Bioresour Technol 311:123584.

Chen L, Zhang H, Zhang L, Li W, Fan F, Wu X, Wu X, Lin J (2020b) Cas9 protein triggers differential expression of inherent genes especially NGFR expression in 293T cells. Cell Mol Bioeng 13:61-72.

Chen Y, Jiang D, Chen W, Zhang X, Luan L, Xu J, Su J, Gao F, Ni Z, Wang H, Tan L, Hou Y (2019) 53P- Poor prognostic impact of NTRK2 gene variation in esophageal squamous cell carcinoma. Ann Oncol 30:v15.

Cheng HC, Sun Y, Lai LC, Chen SY, Lee WC, Chen JH, Chen TF, Chen HH, Wen LL, Yip PK, Chu YM, Chen WJ, Chen YC (2012) Genetic polymorphisms of nerve growth factor receptor (NGFR) and the risk of Alzheimer's disease. J Negat Results Biomed 11:5.

Choi D, Li D, Law S, Powell M, Raisman G (2008) A prospective observational study of the yield of olfactory ensheathing cells cultured from biopsies of septal nasal mucosa. Neurosurgery 62:1140-1145.

Ciarochi JA, Liu J, Calhoun V, Johnson H, Misiura M, Bockholt HJ, Espinoza FA, Caprihan A, Plis S, Turner JA, Paulsen JS; PREDICT-HD Investigators and Coordinators of the Huntington Study Group (2018) High and low levels of an NTRK2-driven genetic profile affect motor- and cognition-associated frontal gray matter in prodromal Huntington's disease. Brain Sci 8:116.

Collins A, Ibrahim A, Li D, Liadi M, Li Y (2019) Reconstruction of the damaged dorsal root entry zone by transplantation of olfactory ensheathing cells. Cell Transplant 28:1212-1219.

Copsel SN, Barreras H, Lightbourn CO, Bader CS, Wolf D, Kale B, Alperstein W, Komanduri KV, Levy RB (2020) IL-2/IL-2R, TL1A/TNFRSF25 or their combined stimulation results in distinct CD4+FoxP3+ regulatory T cell phenotype and suppressive function. Biol Blood Marrow Transplant 26:S169.

Cox J, Mann M (2008) MaxQuant enables high peptide identification rates, individualized p.p.b.-range mass accuracies and proteome-wide protein quantification. Nat Biotechnol 26:1367-1372.

Devon R, Doucette R (1992) Olfactory ensheathing cells myelinate dorsal root ganglion neurites. Brain Res 589:175-179.

Dono A, Wang E, Lopez-Rivera V, Ramesh AV, Tandon N, Ballester LY, Esquenazi Y (2020) Molecular characteristics and clinical features of multifocal glioblastoma. J Neurooncol 148:389-397.

Du J, Yuan Z, Ma Z, Song J, Xie X, Chen Y (2014) KEGG-PATH: Kyoto encyclopedia of genes and genomes-based pathway analysis using a path analysis model. Mol Biosyst 10:2441-2447.

Franssen EH, de Bree FM, Verhaagen J (2007) Olfactory ensheathing glia: their contribution to primary olfactory nervous system regeneration and their regenerative potential following transplantation into the injured spinal cord. Brain Res Rev 56:236-258.

Galimberti D, Fenoglio C, Ghezzi L, Serpente M, Arcaro M, D'Anca M, De Riz M, Arighi A, Fumagalli GG, Pietroboni AM, Piccio L, Scarpini E (2019) Inflammatory expression profile in peripheral blood mononuclear cells from patients with Nasu-Hakola disease. Cytokine 116:115-119.

Gredler ML, Patterson SE, Seifert AW, Cohn MJ (2020) Foxa1 and Foxa2 orchestrate development of the urethral tube and division of the embryonic cloaca through an autoregulatory loop with Shh. Dev Biol 465:23-30.

Gu J, Xu H, Xu YP, Liu HH, Lang JT, Chen XP, Xu WH, Deng Y, Fan JP (2019) Olfactory ensheathing cells promote nerve regeneration and functional recovery after facial nerve defects. Neural Regen Res 14:124-131.

Gu M, Gao Z, Li X, Guo L, Lu T, Li Y, He X (2017) Conditioned medium of olfactory ensheathing cells promotes the functional recovery and axonal regeneration after contusive spinal cord injury. Brain Res 1654:43-54.

Guérout N, Derambure C, Drouot L, Bon-Mardion N, Duclos C, Boyer O, Marie JP (2010) Comparative gene expression profiling of olfactory ensheathing cells from olfactory bulb and olfactory mucosa. Glia 58:1570-1580.

Hamdi-Rozé H, Ware M, Guyodo H, Rizzo A, Ratié L, Rupin M, Carré W, Kim A, Odent S, Dubourg C, David V, de Tayrac M, Dupé V (2020) Disrupted hypothalamo-pituitary axis in association with reduced shh underlies the pathogenesis of NOTCH-deficiency. J Clin Endocrinol Metab 105:dgaa249.

Indraswari F, Wong PT, Yap E, Ng YK, Dheen ST (2009) Upregulation of Dpysl2 and Spna2 gene expression in the rat brain after ischemic stroke. Neurochem Int 55:235-242.

Kadwa RA (2020) Novel Mutation in ATP6V1A Gene with Infantile Spasms in an Indian Boy. Neuropediatrics 51:292-294.

Kim J, Choi Y, Ahn M, Jung K, Shin T (2018) Olfactory dysfunction in autoimmune central nervous system neuroinflammation. Mol Neurobiol 55:8499-8508.

Kobayashi Y, Hayashi R, Shibata S, Quantock AJ, Nishida K (2020) Ocular surface ectoderm instigated by WNT inhibition and BMP4. Stem Cell Res 46:101868.

Lazzari M, Bettini S, Franceschini V (2016) Immunocytochemical characterisation of ensheathing glia in the olfactory and vomeronasal systems of Ambystoma mexicanum (Caudata: Ambystomatidae). Brain Struct Funct 221:955-967.

Li M, Zhu Q, Liu J (2020) Olfactory ensheathing cells in facial nerve regeneration. Braz J Otorhinolaryngol 86:525-533.
Li X, Li C, Zhou P, Chen S (2019) Inhibitory effect of icaritin on proliferation, migration, and invasion of human nasopharyngeal carcinoma cell CNE2 by regulating STAT3 activation. Pharmazie 74:685-687.
Lin N, Dong XJ, Wang TY, He WJ, Wei J, Wu HY, Wang TH (2019) Characteristics of olfactory ensheathing cells and microarray analysis in Tupaia belangeri (Wagner, 1841). Mol Med Rep 20:1819-1825.
Love MI, Huber W, Anders S (2014) Moderated estimation of fold change and dispersion for RNA-seq data with DESeq2. Genome Biol 15:550.
Lowry N, Goderie SK, Adamo M, Lederman P, Charniga C, Gill J, Silver J, Temple S (2008) Multipotent embryonic spinal cord stem cells expanded by endothelial factors and Shh/RA promote functional recovery after spinal cord injury. Exp Neurol 209:510-522.
Mackay-Sim A, St John JA (2011) Olfactory ensheathing cells from the nose: clinical application in human spinal cord injuries. Exp Neurol 229:174-180.
Meaburn KJ, Misteli T (2019) Assessment of the Utility of Gene Positioning Biomarkers in the Stratification of Prostate Cancers. Front Genet 10:1029.
Miedzybrodzki R, Tabakow P, Fortuna W, Czapiga B, Jarmundowicz W (2006) The olfactory bulb and olfactory mucosa obtained from human cadaver donors as a source of olfactory ensheathing cells. Glia 54:557-565.
Monfrini E, Straniero L, Bonato S, Monzio Compagnoni G, Bordoni A, Dilena R, Rinchetti P, Silipigni R, Ronchi D, Corti S, Comi GP, Bresolin N, Duga S, Di Fonzo A (2019) Neurofascin (NFASC) gene mutation causes autosomal recessive ataxia with demyelinating neuropathy. Parkinsonism Relat Disord 63:66-72.
Ogata H, Goto S, Sato K, Fujibuchi W, Bono H, Kanehisa M (1999) KEGG: Kyoto Encyclopedia of Genes and Genomes. Nucleic Acids Res 27:29-34.
Pastrana E, Moreno-Flores MT, Gurzov EN, Avila J, Wandosell F, Diaz-Nido J (2006) Genes associated with adult axon regeneration promoted by olfactory ensheathing cells: a new role for matrix metalloproteinase 2. J Neurosci 26:5347-5359.
Pattwell SS, Arora S, Cimino PJ, Ozawa T, Szulzewsky F, Hoellerbauer P, Bonifert T, Hoffstrom BG, Boiani NE, Bolouri H, Correnti CE, Oldrini B, Silber JR, Squatrito M, Paddison PJ, Holland EC (2020) A kinase-deficient NTRK2 splice variant predominates in glioma and amplifies several oncogenic signaling pathways. Nat Commun 11:2977.
Pelisch N, Rosas Almanza J, Stehlik KE, Aperi BV, Kroner A (2020) CCL3 contributes to secondary damage after spinal cord injury. J Neuroinflammation 17:362.
Pellitteri R, Catania MV, Bonaccorso CM, Ranno E, Dell'Albani P, Zaccheo D (2014) Viability of olfactory ensheathing cells after hypoxia and serum deprivation: Implication for therapeutic transplantation. J Neurosci Res 92:1757-1766.
Peng H, Wan CT, Yin D, Ming JH (2009) In vitro isolation and culture of olfactory ensheathing cells from rat olfactory mucosa and olfactory bulbs using modified Nash differential adhesion and arabinosylcytosin method. Zhongguo Zuzhi Gongcheng Yanjiu yu Linchuang Kangfu 13:39-42.
Peng Q, Chen B, Wang H, Zhu Y, Wu J, Luo Y, Zuo G, Luo J, Zhou L, Shi Q, Weng Y, Huang A, He TC, Fan J (2019) Bone morphogenetic protein 4 (BMP4) alleviates hepatic steatosis by increasing hepatic lipid turnover and inhibiting the mTORC1 signaling axis in hepatocytes. Aging (Albany NY) 11:11520-11540.
Ramli K, Aminath Gasim I, Ahmad AA, Hassan S, Law ZK, Tan GC, Baharuddin A, Naicker AS, Htwe O, Mohammed Haflah NH, R BHI, Abdullah S, Ng MH (2019) Human bone marrow-derived MSCs spontaneously express specific Schwann cell markers. Cell Biol Int 43:233-252.
Ramón-Cueto A, Plant GW, Avila J, Bunge MB (1998) Long-distance axonal regeneration in the transected adult rat spinal cord is promoted by olfactory ensheathing glia transplants. J Neurosci 18:3803-3815.
Reshamwala R, Shah M, St John J, Ekberg J (2020) The link between olfactory ensheathing cell survival and spinal cord injury repair: a commentary on common limitations of contemporary research. Neural Regen Res 15:1848-1849.
Romano C, Ferranti S, Mencarelli MA, Longo I, Renieri A, Grosso S (2020) 17p13.3 microdeletion including YWHAE and CRK genes: towards a clinical characterization. Neurol Sci 41:2259-2262.
Sanders CL, Rattinger GB, Deberard MS, Hammond AG, Wengreen H, Kauwe JSK, Buhusi M, Tschanz JT (2020) Interaction between physical activity and genes related to neurotrophin signaling in late-life cognitive performance: The Cache County Study. J Gerontol A Biol Sci Med Sci 75:1633-1642.
Sarper SE, Kurosaka H, Inubushi T, Ono Minagi H, Kuremoto KI, Sakai T, Taniuchi I, Yamashiro T (2018) Runx1-Stat3-Tgfb3 signaling network regulating the anterior palatal development. Sci Rep 8:11208.
Shi L, Chen H, Qin YY, Gan TQ, Wei KL (2020) Clinical and biologic roles of PDGFRA in papillary thyroid cancer: a study based on immunohistochemical and in vitro analyses. Int J Clin Exp Pathol 13:1094-1107.
Śmieszek A, Stręk Z, Kornicka K, Grzesiak J, Weiss C, Marycz K (2017) Antioxidant and anti-senescence effect of metformin on mouse olfactory ensheathing cells (mOECs) may be associated with increased brain-derived neurotrophic factor levels-an ex vivo study. Int J Mol Sci 18:872.
Smith KE, Whitcroft K, Law S, Andrews P, Choi D, Jagger DJ (2020) Olfactory ensheathing cells from the nasal mucosa and olfactory bulb have distinct membrane properties. J Neurosci Res 98:888-901.
Tan Y, Chen L, Li S, Hao H, Zhang D (2020) MiR-384 inhibits malignant biological behavior such as proliferation and invasion of osteosarcoma by regulating IGFBP3. Technol Cancer Res Treat 19:1533033820909125.
Thaxton C, Pillai AM, Pribisko AL, Labasque M, Dupree JL, Faivre-Sarrailh C, Bhat MA (2010) In vivo deletion of immunoglobulin domains 5 and 6 in neurofascin (Nfasc) reveals domain-specific requirements in myelinated axons. J Neurosci 30:4868-4876.
Thomas PD (2017) The gene ontology and the meaning of biological function. Methods Mol Biol 1446:15-24.
Urbini M, Indio V, Tarantino G, Ravegnini G, Angelini S, Nannini M, Saponara M, Santini D, Ceccarelli C, Fiorentino M, Vincenzi B, Fumagalli E, Casali PG, Grignani G, Pession A, Ardizzoni A, Astolfi A, Pantaleo MA (2019) Gain of FGF4 is a frequent event in KIT/PDGFRA/SDH/RAS-P WT GIST. Genes Chromosomes Cancer 58:636-642.
Voronova A D, Stepanova OV, Valikhov MP, Chadin AV, Semkina A S, Abakumov MA, Reshetov IV, Chekhonin VP (2019) Comparison of the efficiency of transplantation of rat and human olfactory ensheathing cells in posttraumatic cysts of the spinal cord. Bull Exp Biol Med 167:536-540.
Wang GY, Cheng ZJ, Yuan PW, Li HP, He XJ (2021) Olfactory ensheathing cell transplantation alters the expression of chondroitin sulfate proteoglycans and promotes axonal regeneration after spinal cord injury. Neural Regen Res 16:1638-1644.
Wang L, Yang P, Liang X, Ma L, Wei J (2014) Comparison of therapeutic effects of olfactory ensheathing cells derived from olfactory mucosa or olfactory bulb on spinal cord injury mouse models. Xi Bao Yu Fen Zi Mian Yi Xue Za Zhi 30:379-383.
Yam PT, Langlois SD, Morin S, Charron F (2009) Sonic hedgehog guides axons through a noncanonical, Src-family-kinase-dependent signaling pathway. Neuron 62:349-362.
Yang YJ, Xia B, Gao JB, Li SY, Ma T, Huang JH, Luo ZJ (2020) Cell culture supernatant of olfactory ensheathing cells promotes nerve regeneration after peripheral nerve injury in rats. Zhongguo Zuzhi Gongcheng Yanjiu 24:3035-3041.
Yao R, Murtaza M, Velasquez JT, Todorovic M, Rayfield A, Ekberg J, Barton M, St John J (2018) Olfactory ensheathing cells for spinal cord injury: sniffing out the issues. Cell Transplant 27:879-889.
Yuan Z, Xiu C, Liu D, Zhou G, Yang H, Pei R, Ding C, Cui X, Sun J, Song K (2019) Long noncoding RNA LINC-PINT regulates laryngeal carcinoma cell stemness and chemoresistance through miR-425-5p/PTCH1/SHH axis. J Cell Physiol 234:23111-23122.
Yue Y, Xue Q, Yang J, Li X, Mi Z, Zhao G, Zhang L (2020) Wnt-activated olfactory ensheathing cells stimulate neural stem cell proliferation and neuronal differentiation. Brain Res 1735:146726.

C-Editor: Zhao M; S-Editors: Yu J, Li CH; L-Editor: Song LP; T-Editor: Jia Y